Thermal Behavior and Morphology of Polyamide 6 Based Multicomponent Blends

S. H. JAFARI,[1] P. PÖTSCHKE,[1] M. STEPHAN,[1] G. POMPE,[1] H. WARTH,[2] H. ALBERTS[2]

[1] Institute of Polymer Research, Hohe Strasse 6, D-01069 Dresden, Germany

[2] Bayer AG, Plastics Business Group, Research and Development Styrenics, D-41538 Dormagen, Germany

Received 19 February 2001; accepted 20 August 2001

ABSTRACT: The thermal behavior and morphology of multicomponent blends based on PA6, polyamide 6 (PA6)/styrene–acrylonitirle copolymer (SAN), PA6/acrylonitrile–butadiene–styrene terpolymer (ABS), and their compatibilized blends with styrene–acrylonitrile–maleic anhydride copolymer (SANMA) were studied using DSC and SEM. The blends were prepared in a twin-screw extruder under similar processing conditions, keeping the PA6 content fixed at 50 wt %. It was found that, in all the blends, the second component had a nucleating effect and improved the overall degree and rate of crystallization of PA6, whereas addition of a compatibilizer slightly diminished these effects and resulted in significant changes in the blend morphology. The nucleating effect and consequent changes in the crystallization behavior was attributed to the presence of SAN, which is a common component in all the blends. The T_g of PA6 in the blends with a cocontinuous morphology, due to the connectivity between the phases, is higher than in the blends with a disperse-type morphology. The compatibilized blends have a lower crystallization rate and nucleation ability with a cocontinuous morphology, whereas the uncompatibilized blends have a higher crystallization rate with a higher nucleation ability and a disperse and/or a coarse cocontinuous morphology.
 J Appl Polym Sci 84: 2753–2759, 2002

Key words: polyamides; blends; reactive extrusion; crystallization; morphology

INTRODUCTION

Multicomponent blends based on polyamide 6 (PA6) have gained tremendous attention in industrial applications owning to the combination of excellent mechanical properties and processability of these blends. Blends of PA6 with acrylonitrile–butadiene–styrene terpolymer (ABS) are being used in applications where a supertough material with high thermal stability, good chemical resistance, and high dimensional stability is required.[1–3] PA6, with its highly polar functional group, is not compatible with ABS; therefore, while blending of these two polymers, a reactive compatibilizer such as styrene–acrylonitrile–maleic anhydride copolymer (SANMA), can be used for improvement of the interfacial properties.[4–13] The *in situ* graft copolymer formation between MA and amine end groups of PA6 (known as the imidization reaction) and the physical interaction between the styrenic groups of SANMA and the styrene–acrylonitrile copolymer (SAN) component of ABS at the interface are responsible for enhancement of the interfacial properties:

Correspondence to: P. Pötschke (poe@ipfdd.de).

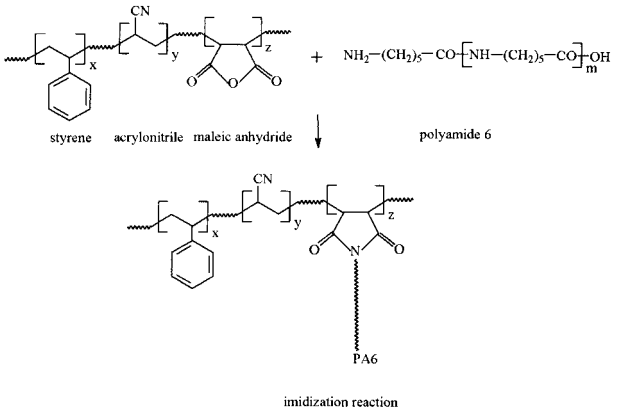

On the other hand, PA6 is a crystallizable polymer and its crystallinity has a direct influence on the ultimate mechanical properties. However, it is known that the crystallinity of a crystallizable polymer in a multicomponent blend system is strongly influenced by the presence of other components.[14–19] Most of the reported works deal with the crystallization behavior in binary blends and/or in nonreactive blends, whereas the crystallization behavior of the reactive multicomponent blends has received less attention because of its complex nature. Since PA6/ABS/SANMA is also a complex multicomponent reactive blend with several components, such as PA6, ABS (SAN-*g*-PB + SAN), and SANMA, it would be easier to study the crystallization behavior of PA6 in model systems with a fewer number of components than in the final system. Therefore, the aim of this work was to study, systematically, the thermal behavior of PA6 in a series of blends starting from a nonreactive binary blend of PA6/SAN to a more complex reactive system such as the PA6/ABS/SANMA blend. The thermal behavior of the PA6 component of the blends was studied by DSC. DSC traces were analyzed and correlated to the changes in nucleation, crystallization rate, and degree of crystallinity. Scanning electron microscopy (SEM) was also used to study the morphology of the blends.

EXPERIMENTAL

All the materials [PA6 Durethan B29, SAN Lustran M80, ABS Novodur Graft (SAN-*g*-PB), and SANMA], supplied by Bayer AG, Dormagen, Germany, were in pellet form except for SAN-*g*-PB, which was delivered in a powder form. These materials were used for melt blending from air-sealed bags without any further treatment. The PA6 used in this work is an intermediate product without any nucleating agent.

The blends were prepared on a ZSK 30 twin-screw extruder (L/D ratio of 41) with simultaneous feeding of all blend components at one feeding point (common melting). Prior to melt blending, SAN and SANMA were dry-blended and fed through a single feeder. The processing temperature of 260°C, feeding rate of 10 kg/h, a unique screw-and-barrel configuration, and screw speed of 200 rpm were used for all the blends' preparation. The melt strands were quenched by passing them through a water bath at room temperature and then were chopped into pellets. Two nonreactive uncompatibilized binary blends, namely, PA6/SAN and PA6/ABS, and two reactive compatibilized ternary blends, namely, PA6/SAN/SANMA and PA6/ABS/SANMA, were made with an identical blend composition (keeping PA6 content constant at 50 wt %). The compatibilizer level was less than 5 wt % of the total blends. In addition to these series of blends, a binary reactive blend of PA6/SANMA was also made under similar processing conditions in which the blending ratio was kept similar to that of the ternary blends. This blend was used to study the individual effect of SANMA on PA6 properties.

Approximately 10 mg of the blend samples cut into small pieces from the granules were used for the DSC studies. The DSC measurements were carried out on a DSC7 Perkin–Elmer (equipped with Pyris-Software, Version 3.51) at heating/cooling rate of $\pm$10 K/min in a N_2 atmosphere in the temperature range from 0 to 250°C. The temperature and transition heat was calibrated by In and Pb standards at a heating rate of 10 K/min. The samples were kept for 1 min at the highest temperature, that is, 250°C, to erase any previous thermal history and then passed through subsequent cooling and heating cycles. The glass transition temperature was determined in the second heat using the inflection point method. The heat of fusion (ΔH_f) in the second heating scan, which is a measure of the degree of crystallization, was used for comparison of the relative changes in the degree of crystallinity. For this purpose, the heat of fusion values were normalized to the PA6 content. Moreover, the ΔT_c values, which are indirectly proportional to the rate of crystallization, were used for the discussion of the influence of blend components on the crystallization rate of PA6, whereas $T_{c,0}$ values were used for comparing the nucleating effect.

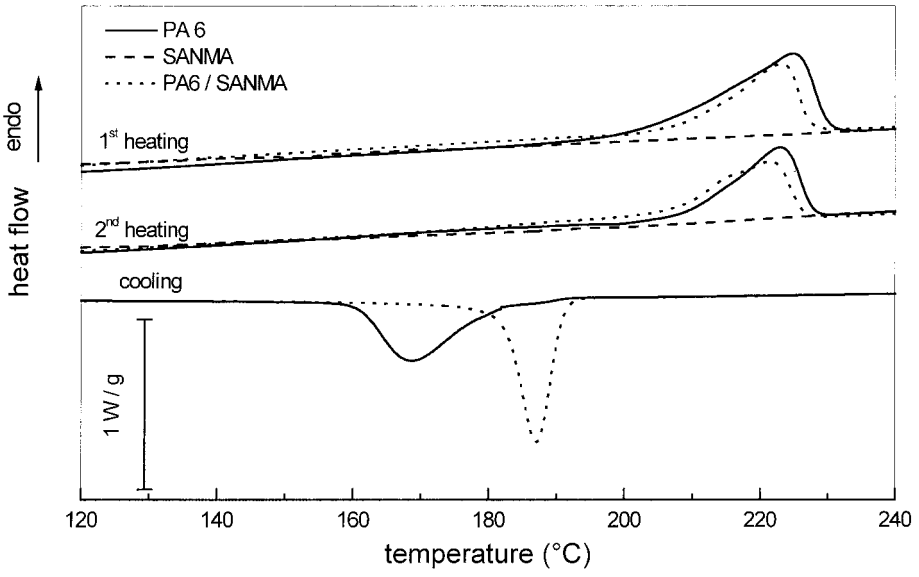

Figure 1 DSC melting endotherms and crystallization exotherm of neat PA6 and its blend with SANMA.

The morphology of the blends was studied by scanning electron microscopy (SEM). The extruded blends in a granulated form (approximately 5 mm long) were used for the morphological characterization. The smooth surface, obtained using a steel knife on a rotational microtome (Jung RM 2055, Leica, Germany) at room temperature, was etched in formic acid for 4 h to remove the polyamide content of the blends. For the PA6/SAN binary blend THF was used for 24 h to dissolve the SAN component of the blend, because, in this blend, SAN was the disperse phase. The etched surface, after proper drying, was gold-sputtered and observed under a LEO 435 VP, UK scanning electron microscope. The scale in the micrographs is 10 μm.

RESULTS AND DISCUSSION

The heating and cooling scans normalized to the PA6 content in the blend are plotted for neat PA6 and its binary reactive blend with SANMA in Figure 1. The characteristic data (heat-transition temperature) are summarized in Table I. It can be seen that the neat PA6 shows a broad melting endotherm in the temperature range of 190–230°C with a peak temperature of 223–225°C. The corresponding crystallization exotherm peak temperature $T_{c,m}$ is about 169°C, with the extrapolated temperature $T_{c,0}$ of 181°C. The changes of the PA6 behavior in the PA6/SANMA blend are more prominent in the crystallization exotherm. SANMA has a strong nucleating effect for the PA6 crystallization. Although the PA6/SANMA blend should be a reactive blend, in which the MA group of SANMA reacts rapidly with the amine end groups of PA6, no change of the glass transition of both components could be observed (see Table III). This might be due to the relative small amount of MA in the entire blend. The main effect of SANMA is the nucleating activity connected with a high nucleation rate and higher crystallization than that of PA6. A similar analysis was also performed for PA6/SAN and PA6/ABS blends and the results are given in Figure 2 along with a comparison between the blend morphologies.

Generally, it can be seen that all the blends show a significant increase in nucleation ability, degree of crystallinity, and crystallization rate of PA6. However, there are slight variations within the blends, which can be attributed to the role of each individual blend component and their possible physical and/or chemical interactions. The observed high nucleation effect could be due to that the used PA6 was an intermediate product and, unlike the commercial products, did not contain any additives in the form of nucleating agents or stabilizers. It seems that the nucleation effect is due mainly to the SAN component of the blends, since this effect is the highest for PA6/SAN, whereas this is slightly lower for the PA6/ABS and PA6/SANMA blends. In the latter blends, a small portion of SAN is replaced by

Table I Characteristic Values of Crystallization and Melting Behavior of PA6 and the Blends

	Heating				Cooling			
	T_m (°C)		ΔH_f (J/g$_{PA6}$) (160–235°C)					
Samples	1st Heat	2nd Heat	1st Heat	2nd Heat	ΔH_c (J/g$_{PA6}$) (120–200°C)	$T_{c,m}$ (°C)	$T_{c,0}$ (°C)	ΔT_c (K)
PA6	224.9	222.8	94.4	62.2	−62.3	168.8	181.0	12.2
PA6/SAN	223.9	221.4	66.1	72.0	−73.2	189.6	193.0	3.4
PA6/ABS	222.3	221.7	57.5	65.2	−63.9	190.3	194.4	4.1
PA6/SANMA	222.7	221.4	64.7	70.1	−68.8	187.1	191.0	3.9
PA6/SAN/SANMA	224.1	211/220.8	74.1	69.3	−68.6	179.4	187.0	7.6
PA6/ABS/SANMA	222.5	215/221.7	57.5	68.9	−69.8	186.8	191.6	4.8

The transition heats are normalized to the PA6 content in the blends.

a bulky graft polymer (SAN-*g*-PB) in ABS or by a reactive comonomer (SAN-*co*-MA) in SANMA. In the ternary blends, further replacement of SAN with the compatibilizer (SANMA) results in a greater decrease of the nucleation effect. Similarly, increase in the rate and degree of crystallinity of PA6 in the blends is also highest for the PA6/SAN blend, whereas it is less effective for the other blends. Therefore, in all these blends, SAN plays a more major role in controlling the crystallization behavior of PA6 than that of any other component.

Changes in the crystalline phase of PA6 as a result of blending are also accompanied by changes in the amorphous phase. The T_g of the PA6 component of the blends at 54°C shifts to a higher temperature, whereas the T_g of the second component remains almost unchanged in the blends at 110°C (Table II). This shows that the second component of the blends causes some restriction in the molecular mobility of the PA6 chains. This effect is much more pronounced for PA6/ABS as compared to the ternary blends, whereas no changes in the T_g were observed for the PA6/SAN and PA6/SANMA blends. This indicates that the presence of SAN or the chemical reaction between SANMA and PA6 alone are not

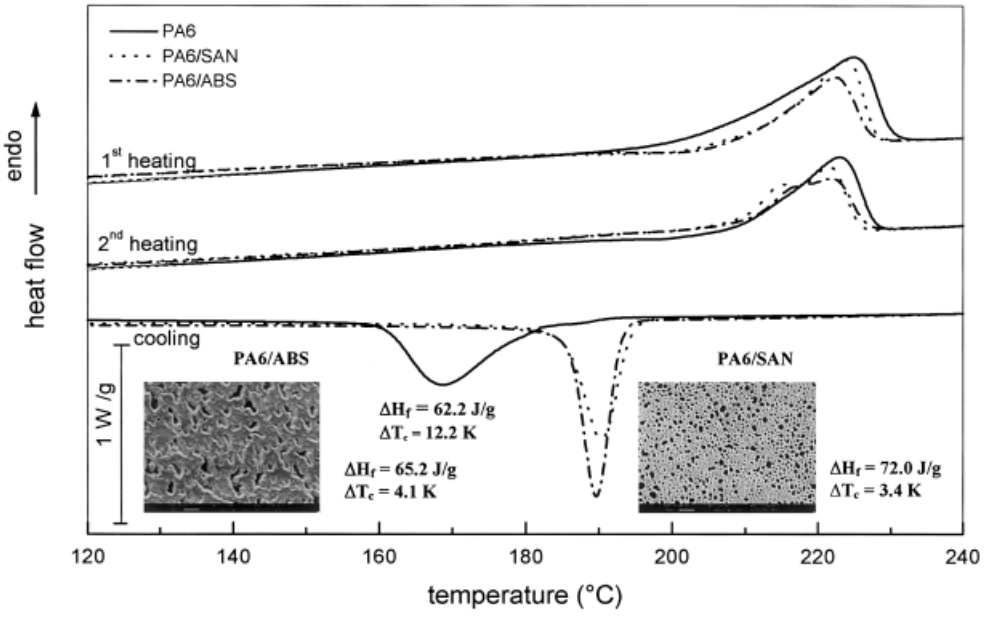

Figure 2 DSC traces of PA6/SAN and PA6/ABS nonreactive binary blends.

Table II Glass Transition Temperature of the Neat Polymers and the Blends

	T_g (°C)			
Samples	PA6	SAN	ABS	SANMA
PA6	54	—	—	—
SAN	—	110	—	—
ABS	—	—	109	—
SANMA	—	—	—	109
PA6/SANMA	54	—	—	109
PA6/SAN	54	110	—	—
PA6/SAN/SANMA	58	110	—	109
PA6/ABS	60	—	109	—
PA6/ABS/SANMA	57	—	109	109

responsible for the observed increase in the T_g of PA6 in the blends. Apparently, the SAN-*g*-PB component of ABS and the combined chemical and physical interactions between the blend components mainly cause the observed changes in the amorphous phase of PA6.

DSC traces along with relevant blend morphologies for the ternary compatibilized blend of PA6/SAN/SANMA and PA6/ABS/SANMA and the binary uncompatibilized blends are shown in Figures 3 and 4, respectively. The corresponding data are listed in Table I. The blends show a wide range of morphology spectra from a disperse type in PA6/SAN to a coarse cocontinuous morphology in PA6/ABS and a fine cocontinuous morphology in the compatibilized blends. The SANMA terpolymer acts as an effective compatibilizer for these blends. The *in situ* graft polymer formation at the PA6–SANMA interface and, on the other hand, the physical interaction between styrenic groups of SAN and SANMA result in a reduction of the interfacial tension and formation of a cocontinuous morphology. This compatibilization process is also effective for PA6/ABS/SANMA. This blend has the finest cocontinuous morphology among all these blends

Comparison of the crystallization behavior between the nonreactive binary blends and the reactive ternary blends indicates that the ternary compatibilized blends have a slightly hindered crystallization behavior and a lower T_g than those of the binary blends. However, the PA6/ABS/SANMA blend shows a slight improvement only in the degree of crystallization as compared to the PA6/ABS blend. The PA6/SAN/SANMA has a higher T_g than that of the uncompatibilized PA6/SAN blend. The possible reason for these exceptional behaviors could be the significant changes in the blend morphologies. PA6 blends with ABS have cocontinuous morphologies with finer phase dimensions for the compatibilized blend than those of the uncompatibilized blend, whereas the compatibilization in blends of PA6 with SAN led to a sudden change from a dispersed-type morphology to a cocontinuous morphology.

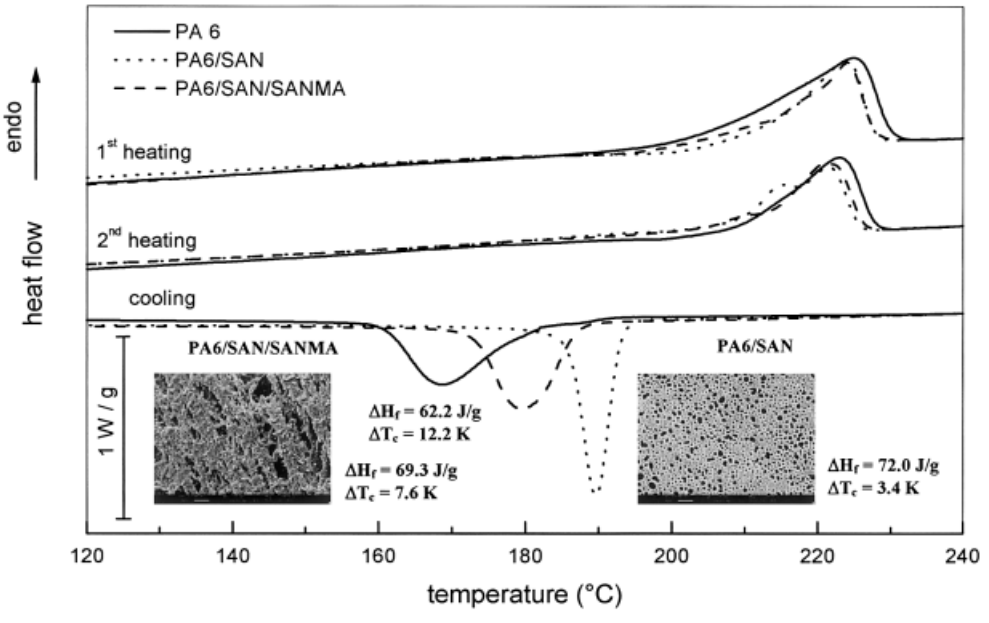

Figure 3 DSC traces and morphology of PA6/SAN/SANMA reactive ternary blends.

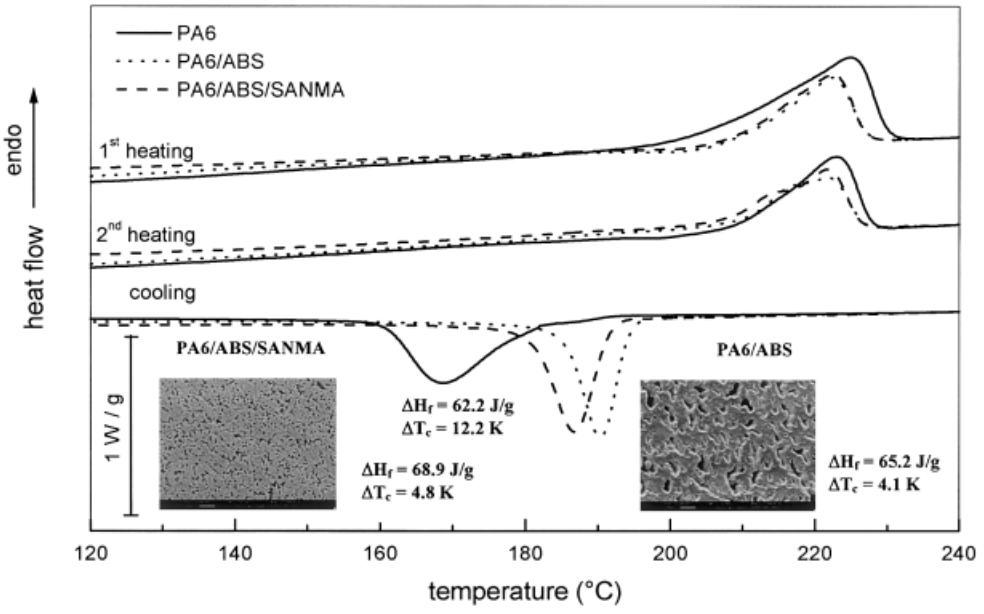

Figure 4 DSC traces and morphology of PA6/ABS/SANMA reactive ternary blends.

Hence, in summary, it can be stated that compatibilized blends have a lower crystallization rate and a lower nucleation ability with a cocontinuous morphology, whereas the uncompatibilized blends have a higher crystallization rate with a higher nucleation ability and have a disperse or a coarse cocontinuous morphology. The T_g of PA6 in the blends with a cocontinuous morphology, due to the connectivity between the phases, is higher than that of the blend with a disperse-type morphology.

CONCLUSIONS

The effect of reactive and nonreactive blending and the blend components on the crystallization and melting behavior as well as the glass transition behavior of PA6 in a series of multicomponent blends, namely, PA6/SAN, PA6/ABS, PA6/SANMA, PA6/SAN/SANMA, and PA6/ABS/SANMA, were studied using DSC and SEM. The individual effect of each component, their combined effect, and the resulting possible interactions in the form of chemical reactions and or the physical interaction between similar groups on the PA6 properties were discussed systematically. It was found that in all the blends the second component had a nucleating effect and improved the overall degree and rate of crystallization of PA6, whereas addition of the compatibilizer slightly diminished these effects and resulted in significant changes in the blend morphology. The nucleating effect and consequent changes in the crystallization behavior was attributed to the presence of SAN, which is a common component in all the blends. These changes in the crystallization behavior were also supported by changes in the amorphous region. The T_g of PA6 in the blends with a cocontinuous morphology due to the connectivity between the phases is higher than that of the blends with a disperse-type morphology. The compatibilized blends have a lower crystallization rate and nucleation ability with a cocontinuous morphology, whereas the uncompatibilized blends have a higher crystallization rate with a higher nucleation ability and have a disperse and/or a coarse cocontinuous morphology.

REFERENCES

1. Dunning L. Kunststoffe 1996, 86, 98–100.
2. de Clercq Zubli, M.; Verhooren, P. Kunststoffe Plast Eur 1997, 87(12), 19–20.
3. Henton, D. E.; Mang, M. N. U.S. Patent 5 089 557, Feb. 18, 1992.
4. Kudva, R. A.; Keskkula, H.; Paul, D. R. Polymer 2000, 41, 239–258.
5. Kudva, R.A.; Keskkula, H.; Paul, D. R. Polymer 1998, 39, 2447–2460.

6. Majumdar, B.; Keskkula, H.; Paul, D. R. Polymer 1994, 35, 4263–4279.
7. Majumdar, B.; Keskkula, H.; Paul, D. R. Polymer 1994, 35, 5453–5467.
8. Triacca, V. J.; Ziaee, S.; Barlow, J. W.; Keskkula, H.; Paul, D. R. Polymer 1991, 32, 1401–1413.
9. Lacasse, C.; Favis, B. D. Adv Polym Tech 1999, 18, 255–267.
10. Majumdar, B.; Keskkula, H.; Paul, D. R. Polymer 1994, 35, 3164–3172.
11. Misra, A.; Sawhney, G.; Kumar, R. A. J Appl Polym Sci 1996, 62, 1395–1405.
12. Horak, Z.; Krulis, Z.; Fortelny, I. Polym Networks Blends 1997, 7, 43–49.
13. Cho, K.; Seo, K. H.; Ahn, T. O. Polym J 1997, 29, 987–991.
14. Jafari, S .H.; Gupta, A. K. J Appl Polym Sci 2000, 75, 1769–1775.
15. Jafari, S. H.; Gupta, A. K. J Appl Polym Sci 1999, 71, 1153–1161.
16. Hage, E.; Ferreira, A. S.; Manrich, S.; Pessan, L. A. J Appl Polym Sci 1999, 71, 423–430.
17. Psarski, M.; Pracella, M.; Galeski, A. Polymer 2000, 41, 4923–4932.
18. Eersels, K. L. L.; Groeninckx, G. J Appl Polym Sci 1997, 63, 573–580.
19. Ou, Y.-C.; Si, M.-Y.; Yu, Z.-Z. J Appl Polym Sci 1999, 73, 767–775.